peak sites and new atoms positioned at the bcc pit sites.

- The number of peaks, passes, pales, and pits in a unit cell (i.e., in a 3-torus $S^1 \times S^1 \times S^1$) obeys the Euler-Poincare relationship for Euclidean space, i.e., peaks - passes + pales - pits = 0, and the following Morse inequalities:

  pits ≥ 1
  peaks ≥ 1
  pales - pits ≥ 2
  passes - peaks ≥ 2
  passes - pales + pits ≥ 1
  pales - passes + peaks ≥ 1
- The inequalities are too weak to be of much value in practice; thus, there is a definite need for much stronger inequalities that incorporate space group specific invariants based on equivariant topology and can be applied to the wrapped-up asymmetric unit (i.e., orbifold) rather than the wrapped-up unit cell (i.e., 3-torus cover).
- The total number of critical points of a given type belonging to an asymmetric unit (fundamental domain) of a crystallographic unit cell can be calculated by dividing the sum of Wyckoff site multiplicities for all sites occupied by critical points of that type by the Wyckoff site multiplicity for the general position site. For simple high symmetry structures, this number is often less than one.
- Since the Betti numbers for the 3-torus are 1,3,3,1, the minimum number of critical points possible in a crystallographic unit cell is 8, (i.e., 1,3,3,1 in P$\overline{1}$ with critical points on the 8 inversion centers). Betti numbers are topological invariants used in the derivation of the Morse inequalities.[2,3,5]
- The inequalities are still of little practical value; thus, there is a definite need for much stronger inequalities that incorporate space group specific invariants based on equivariant topology and can be applied to the wrapped-up asymmetric unit (i.e., orbifold) rather than the wrapped-up unit cell (i.e., 3-torus).

4. Critical Nets on Orbifolds

In Sect 3. we saw that critical net drawings can become rather complex even for very simple examples such as the body-centered cubic (bcc) structure. In the present section, we introduce critical nets on orbifolds, which reduce both the graphical and interpretation complexity associated with critical nets while including valuable space group topology information as well.

4.1 Body-Centered Cubic Orbifold

The orbifold for Im$\overline{3}$m, the parent space group for bcc structures, is derived from the fundamental domain shown in the lower left of Fig. 4.1. The space group coordinates for the vertices of the fundamental domain are given in parentheses as fractions of the unit cell lengths. The arrows denote the down density critical net paths leading from the peak at (a) to the pit at (b). Wyckoff identification letters (a-k) are shown on the asymmetric unit drawing, and the ITCr[1] information on most of those Wyckoff sites is listed in the columns labeled "Wyckoff Set" in the middle of the figure. The tetrahedral fundamental domain has three sides bounded with the top (k) and bottom (j) mirrors with (k) bridged over the 3-fold axis as described in Sect. 1.6, but the fourth side is open (unbounded) with a 2-fold axis (i) extending from one corner of the open end (c) to the center (d) of the opposite face, which contains another 2-fold axis (g).

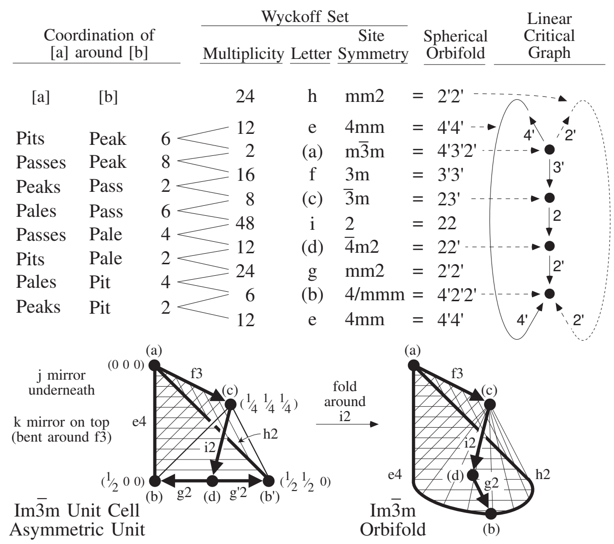

Figure 4.1. Construction of Im$\overline{3}$m orbifold from asymmetric unit and superimposition of body-centered cubic lattice complex to form linear critical graph.

Visualize the tetrahedral asymmetric unit as a single-pole pup tent, covered by a silvered rubber reflective sheet, with a support pole (i) in the entrance. A horizontal "threshold" pole (g) with a hinge in the middle (d) lies across the front of the tent floor with the hinge attached to the bottom of the support pole. To close the tent, we grab the two corners of the rubber sheets (j and k) at the two ends (b) and (b') of the hinged threshold pole (g) and bring them together stretching the extensible and flexible tent floor poles (e) and (h) in the process. We then zipper the edges of the sheet (k) together to form the bounded orbifold shown in the lower right drawing of Fig. 4.1.

The underlying topological space of this 3-orbifold is a 3-ball. Using the notation in Fig. 2.3, the orbifold has two singular points of type j, 4'3'2' at (a) and 4'2'2' at (b), and two singular points of type i, 23' at (c) and 22' at (d).

4.2 Linearized Critical Nets on Orbifolds

Critical nets are actually Morse functions that are defined in terms of a mathematical mapping from Euclidean 3-space to Euclidean 1-space (i.e., a single valued 3-dimensional function). Taking this requirement literally, we deform the orbifold so that the Euclidean 1-space of density is vertical in the page (i.e., peak height > pass height > pale height > pit height). This adds a welcome constraint to the drawing of orbifolds that in general have no inherent topological constraints to guide the illustrator. The topologist would probably tend to draw it as a solid sphere, but we are not violating any topological principles in forming the linearized critical net on orbifold (i.e., linear critical graph) shown at the top of Fig. 4.1.

The multiplicity for each Wyckoff site is given as a column in the table and the preceding column shows the integer ratios of the multiplicities in adjacent rows, which are by design the adjacent elements in the critical net graph. These ratios tell us the coordination numbers of critical net components around other critical net components, thus summarizing much of the structural topology information you would obtain by examining ORTEP-III critical net stereo drawings or calculating and evaluating long tables of intercomponent distances and angles. Note the abbreviated orbifold critical set notation in the linear critical graph of Fig. 4.1 where 3'3' becomes 3', and stationary points such as 4'3'2' are denoted by the labels on the lines intersecting at that point.

4.3 Resolution of the Critical Net Versus Tiling Discrepancy

The coordination numbers also provide a method for applying topological constraints in that there must be exactly two peaks around a pass and two pits around a pale. This particular combinatorial constraint holds for the tiling approach of Dress, Huson, and Molnár[34] as well as for our critical net Morse function approach. Fig. 4.2 shows two solutions satisfying that constraint based on the orbifold topology for space group $Fd\bar{3}m$ with atoms (i.e., tiling vertices in the Dress approach, peaks in the critical net approach) on the two $\bar{4}3m$ sites of $Fd\bar{3}m$. Fig. 4.2 compares the two configurations assuming both are linearized critical nets on the $Fd\bar{3}m$ orbifold. The columns of numbers are sums of Wyckoff set multiplicities for each level of the critical net and integer ratios of neighboring rows. Only the connections between adjacent levels are summed. An ORTEP drawing of the configuration labeled bcc derivative is shown in Fig. 3.4. A similar drawing cannot be made for the special rhombohedral tiling given by the second configuration since the two pales are far from collinear with the pit.

What's going on here? First, we note that the left configuration has seven nodes while the right has only six, but the six in common are on the same Wyckoff sites and point positions. We then note that on the orbifold drawing, in the lower right of the figure, the h2 axis lies directly between the (e) and (f) sites. Since a separatrix line can never traverse more than one isometry zone (i.e. Wyckoff site zone), there has to be another critical point at point (h). According to the special rhombohedral indexing, this point would have to be a degenerate critical point with a cubic (triple point) algebraic dependence rather than quadratic along the (e) to (f) vector since the density is heading downhill along that vector. We can always decompose a degenerate critical point into several nondegenerate critical points, but then we would be in trouble satisfying the Euler-Poincare relationship described in Sect. 3.10. The obviously related (c) and (d) Wyckoff sites must be assigned to the same Morse function levels, which then produces the correct configuration shown in the left-hand drawing.

In other situations, missed critical points may make one of the critical points found appear to be degenerate. In our experience to date, a critical net that is not a Morse function has always been traceable to misindexing caused by the omission of valid critical points. Once the peak positions have been assigned by positioning atoms and assigning their Gaussian thermal motion parameters, the rest of the critical net is fixed; it is just a case of determining what it is. In the simple structures we are discussing in this treatment, the thermal motion probability density is either constrained by symmetry to be isotropic or assumed to be isotropic and in any case has little effect on critical net details. Thus we omit smearing functions from the discussion other than to say they are isotropic, Gaussian, and mildly overlapping.

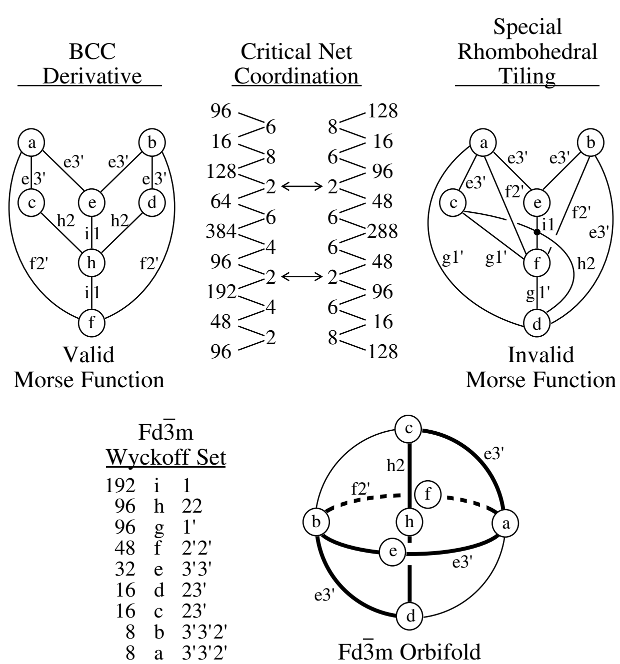

Figure 4.2. Comparison of critical net and tiling results.

5. Lattice Complexes on Critical Nets on Orbifolds

Critical nets on orbifolds, as presented in Sect. 4, provide a wealth of local topology information about the parent space group and simple structures on that space group. The global topology information is also there, encoded in the macrodetails of the combined critical net graph and orbifold, but sometimes we need a more specific summary of the global picture. A simple example concerns the difference between face centered cubic (fcc) and hexagonal closest packing (hcp) which have identical substructures as indicated by the coordination vector as shown in Figs. 5.2 and 5.4. Lattice complexes are convenient for the next step up past the coordination vector. In fact, the fcc and hcp configurations have their own lattice complex symbols F and E, respectively.

5.1 Lattice Complex Background

Lattice complexes have over a 75 year history in crystallography. We find much of the literature on lattice complexes more complex than we need for our application, but there is an introductory paper[40] that describes the basics we use. Once those basics are understood, certain key tabulations in Fischer, Burzlaff, Hellner, and Donnay;[41] Koch;[42] and Fischer and Koch[43] become useful. The definition given in the most recent reference[43] is that a lattice complex is the set of all point configurations that may be generated within one type of Wyckoff set. Hellner's definition[40] is that a lattice complex is an arrangement of equivalent points (or equipoints) that are related by space group symmetry operations, including lattice translations. Example applications of lattice complexes are given by Hellner, Koch, and Reinhardt.[44]

The "characteristic space-group type" of a lattice complex is defined as the highest symmetry space group that can generate the lattice complex. All other space groups with the same lattice complex are subgroups of that characteristic space group, but not all the subgroups contain the lattice complex (i.e., being a subgroup is a necessary but not sufficient condition). For lattice complex I, the characteristic space-group type is Im$\bar{3}$m; and the "characteristic space-group site" is m$\bar{3}$m at Wyckoff position a in space group Im$\bar{3}$m, which is a fixed point with zero degrees of freedom.

5.2 Lattice Complex Notation

Any lattice complex that has its characteristic space-group site on a fixed point is called an invariant lattice complex. Those with one degree of freedom are called univariant lattice complexes, etc. Among the 36 invariant lattice complexes, 11 are rotational or stereometric isomers of others. The remaining 25 listed in order of the number of points [n] per cell in a lattice complex are: [1] P; [2] C, E, G, I; [3] J, N, +Q, R; [4] vD, F, +Y; [6] J*, W; [8] D, vT, +Y*; [9] M; [12] S, +V, W*; [16] T, Y**; [24] S*, V*. The lattice complex W* for example is called a twelve pointer. All the points are on an 8×8×8 sublattice within the unit cell (12×12×12 sublattice for hexagonal unit cell). Those equivalent to Bravais lattices are P, C, I, R, and F.

In Figs. 2.8, 5.1, 5.2, 5.3, 5.4, and A1, the lattice complex symbols with subscript 2, ab, or c denote cell doubling in three, two, or one dimension(s). A superscript digit (1, 2 or 3) denotes the positional degrees of freedom for sites not on fixed points.

Lattice complexes (LC) provide convenient nomenclature, classification, and data management representations for space-group orbifolds and critical nets. As an example, the 3-orbifold I$\bar{4}$3m (#217), shown in Appendix Fig. A.1, is described in our extended Wyckoff notation as:

```
 2-a-3'3'2'-     [I]
 6-b-22'-        [J*]
 8-c-3'3'-    ae:[(I4)3'{P^1_2}3'&]
12-d-20-         [W*]
12-e-2'2'-    ab:[(I6)2'(J*2)]
24-f-22-      bd:[(J*4)2(W*2)]
24-g-1'-      ec:[(I6)2'(J*2)+((I4)3'{P^1_2}3'&)]1'
48-h-1-       fg:[f(d@RP^2)+g@D^2]@D^3
```

where (a,b,d), (c,e,f), (g) and (h) are invariant, univariant, divariant, and trivariant LC, respectively. The structuring (pq:) is hierachical with invariants in univariants, invariants and univariants in divariants, etc.

The most general LC (the trivariant LC (h) in this example) describes the total orbifold, or if no singular set is present, the manifold. In (h) the underlying 3-ball (D^3) topological space has a mirror 2-disk boundary (D^2), containing (g), and a single suspension RP^2 antipodal surface representation with cone point (12-d-20) and cone axis (24-f-22). The univariant LC notation for (8-c-3'3'), (12-e-2'2'), and (24-f-22) includes coordination numbers from Wyckoff multiplicity ratios as calculated in Fig. 4.1. The notation [(I4)c3'(P_2^1)3' &] in (c) describes a site on the 3'-axis called an invariant limiting lattice complex.[41,43,45] {P_2^1} (which has the multiplicity of the 3'-axis site (c) on which it lies). The 3'-axis then loops back (denoted by &) to the starting point (2-a-3'3'2') through a second ((I4)3') connection. All limiting lattice complexes are omitted from 3-orbifold Figures 2.8 and A.1, but several univariants are included in Figures 5.1-5.4.

5.3 Lattice Complex Splitting Equations

The lattice-complex splitting equations[40,41] for the cubic lattice complexes interrelate the lattice complexes. These include F=P+J, P_2=I+J*, W_2=V*+S*, I=P+P", P_2=F+F", J*=J+J", W*=W+W", D=F+F', D"=F"+F"', I_2=D+D", V*=${}^{+}$V+${}^{-}$V, S*=S+'S, F_2(@ 1/8,1/8,1/8)=T+T", I_2=P_2+P_2', Y**=${}^{+}$Y*+${}^{-}$Y*, ${}^{+}$Y*=${}^{+}$Y+${}^{+}$Y", and ${}^{-}$Y*=${}^{-}$Y+${}^{-}$Y" with ', ", and "' denoting translations along a body diagonal by (1/4,1/4,1/4), (1/2,1/2,1/2), and (3/4,3/4,3/4), respectively. In our analysis of critical nets, these equations relate a lattice complex in one net to a path between two lattice complexes in a net at a lower level. In Fig. 5.1, for example, the P_2 lattice complex in Im$\bar{3}$m is related to the two F lattice complexes in Pn$\bar{3}$m and the 3-fold path between them by P_2=F+F".

5.4 BCC Symmetry Breaking Family

In order to point out some additional properties about orbifolds and critical nets on orbifolds, we examine a series of related cubic space group orbifolds that accommodate the body-centered cubic critical net. The series of cubic space group orbifolds that are related by group/subgroup relationships starting with Im$\bar{3}$m is shown in the linearized critical nets of Fig. 5.1, which includes the cesium chloride and body-centered cubic critical net crystal structure types.

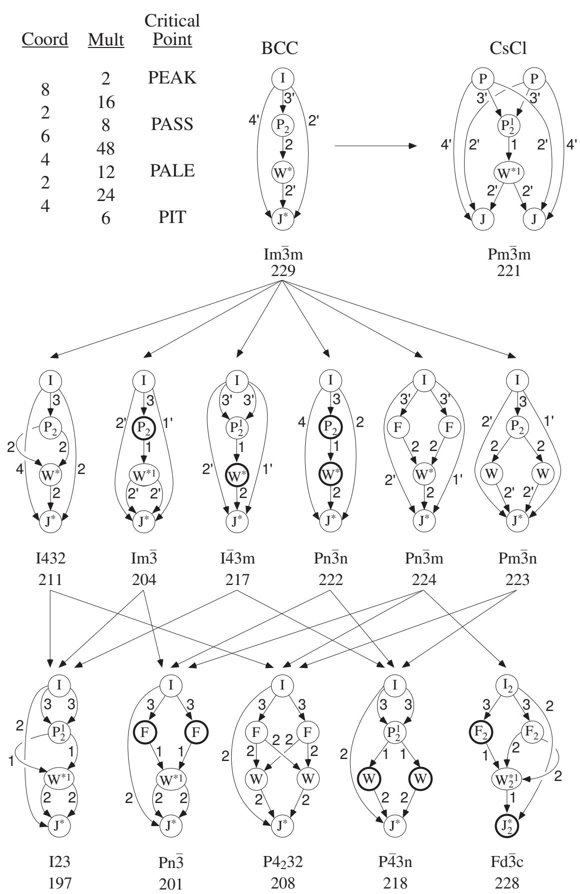

Figure 5.1. Body-centered cubic and CsCl critical nets superimposed onto cubic space group orbifolds.

Notes on orbifold Figs. 5.1, 5.2, and 5.3:

- A straight arrow between graphs points toward a normal subgroup, a straight arrow within a graph points toward a site of "lower density", an arrow between adjacent levels within a graph indicates a critical net Morse function separatrix, and an arrow between nonadjacent levels within a graph indicates a symmetry axis of the space group orbifold that is not embedded into the critical net Morse function.
- A number greater than 1 labeling a line of a graph indicates a 2-, 3-, 4-, or 6-fold crystallographic rotation axis while 1 indicates a path within a general position zone.
- A primed number indicates the path lies in a mirror.
- A thick circle indicates a projective plane suspension point arising from an inversion point not in a mirror (i.e., types b and e of Fig. 2.3).
- For a group/subgroup pair, each axis within the parent graph is either split into two identical axes or reduced in group order by one half (e.g., 4' → 4' + 4', 4' → 4, or 4' → 2') in the subgroup graph.
- A superscript number on a lattice complex symbol denotes the degree of positional freedom at that site.
- Mult, the sum of Wyckoff multiplicities for a row of elements in a graph, is the same for all groups in the illustration except Fd$\bar{3}$c (#228), which has 8 times that number because of its multiple cell (e.g., I → I_2) lattice complexes.
- Integer ratios of adjacent multiplicities provide the coordination vector.
- The odd-order 3-fold axis in an orbifold is the only operator that can:
  - Continue through a 332 or 3'3'2' junction
  - Bridge a mirror over itself without breaking the mirror if it is 3'3'
  - Permit a 2-fold axis to continue through a 322 or 3'2'2' junction

  In other words, separate edges of a graph can represent different segments of the same Wyckoff site if a 3-fold axis is present.

Notes specific to Fig. 5.1:

- By adding the shortest peak-to-pit path (4' for #229) to the graph, we also obtain the number of peaks around pits (2) and pits around peaks (6) as coordination numbers. The extended coordination vector [e.g., (6)(8,2,6,4,2,4)(2) for bcc] can be used as a local topological description of critical net coordination topology for simple critical nets.
- The underlying topological spaces for Fig. 5.1 are the 3-ball in #229, #221, #224, and #223; S^3 in #211 and #208; RP^3 in #197; doubly suspended RP^2 in #222, #201, #218, and #228; and 3-ball plus singly suspended RP^2 in #204 and #217.

5.5 Additional Cubic Space Group Examples

The face-centered cubic and the diamond families are shown in Figs. 5.2 and 5.3, respectively.

Coord	Mult	Critical Point
	4	PEAK
12	48	
2	24	PASS
4	96	
3	32	PALE
2	32+32	
8,4	4+8	PIT

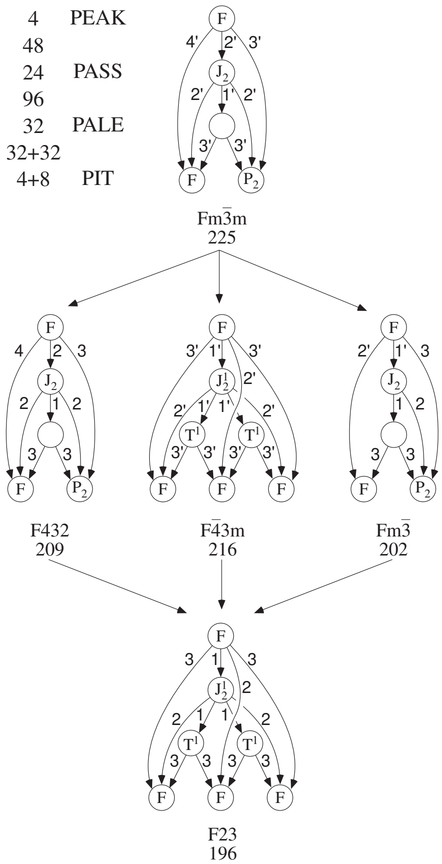

Figure 5.2. Face-centered cubic critical net superimposed onto cubic space group orbifolds.

See “Notes on orbifold Figs. 5.1, 5.2, and 5.3” following Fig. 5.1.

Notes specific to Fig. 5.2:

- Graph nodes that are blank (i.e., without a lattice complex descriptor) are still lattice complexes but do not have a parent on an invariant fixed position and thus do not have a standard crystallographic name.
- The 3' axis in orbifold #216 and the 3-fold axis in #196 extend through all four F lattice complexes, 3'3'2' and 332, respectively, to form loops.
- A single mirror covers orbifold #216.
- The underlying topological spaces are the 3-ball in #225, #216 and #202 and the 3-sphere in #209 and #196.

Coord	Mult	Critical Point
	8	PEAK
4	32	
2	16	PASS
6	96	
6	16	PALE
2	32	
4	8	PIT

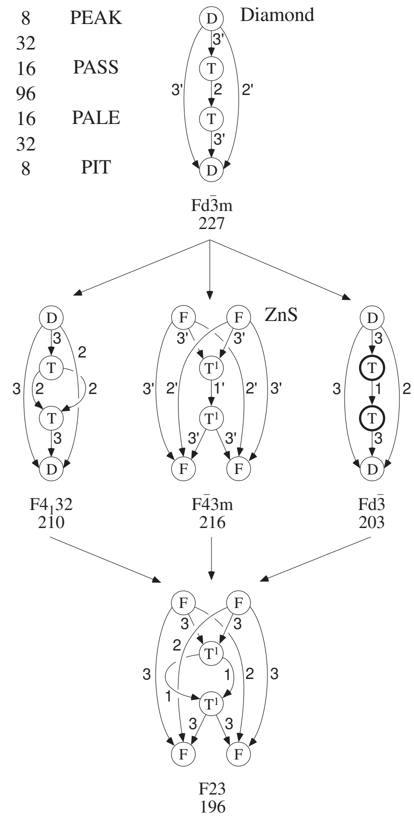

Figure 5.3. Diamond and ZnS critical nets superimposed onto cubic space group orbifolds.

Note specific to Fig 5.3:

- The underlying topological spaces are the 3-ball in #227 and #216, the 3-sphere in #210 and #196, and the doubly suspended projective plane in #203.

5.6 Hexagonal Space Group Examples

Fig. 5.4 shows the critical nets for graphite, hexagonal diamond, and hcp, which all crystallize in the same hexagonal space group, P6_3/mmc. The Wyckoff set and orbifold for that space group also are shown.

The nodes of the critical net graphs in Fig. 5.4 contain the appropriate Wyckoff symbol rather than the lattice complex symbols. The Wyckoff to lattice complex mapping is a,b → Pc; c,d → E; and g → N, where Pc stands for primitive with doubling along the c axis.

The upper left drawing of Fig. 5.4 is the orbifold that has a single 2' axis, h, extending around the upper edge of the kitchen measuring-scoop shaped basin. There are three 3' axis intersections (b, c, & d) that h traverses to form a complete loop. The leading end of the scoop has a single 3' axis half-loop, f, while the support spine along the back of the scoop is a second 3' axis, e. The bottom point, a, at the spine, e, gives rise to a 2 axis that goes through open space from point a to point g in the forward end of the scoop. Everything below the 2' axis, h, is covered by mirror floor, k, while that above h has a mirror ceiling, j.

The hcp critical net in the upper right has the multiplicities shown for each critical net component and the coordination vector (8)(12;2;4;3;2;8,4)(6,1), which is identical to that for fcc in Fig. 5.2. The summed hcp multiplicities are all smaller than those for fcc by a factor of two because of the supercell in fcc caused by repeating after three layers in fcc versus two layers in hcp.

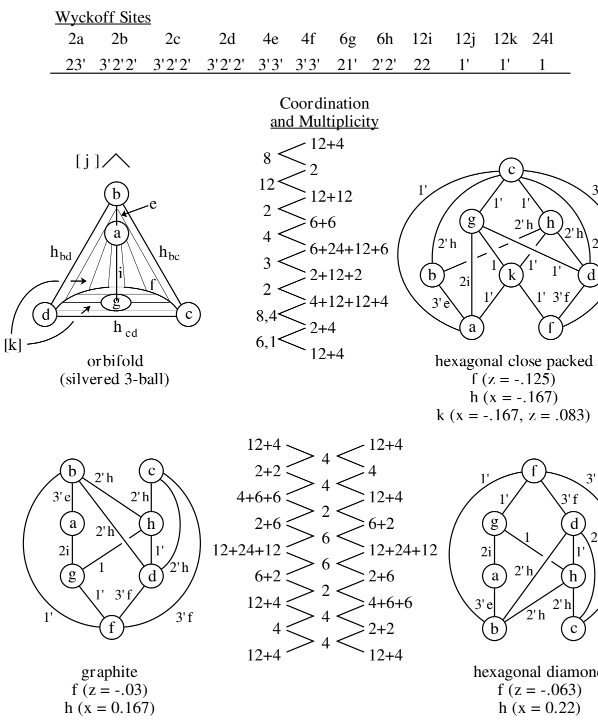

Figure 5.4. Three different critical nets on the hexagonal space group P6$_3$/mmc orbifold.

An interesting feature of critical nets is duality in which the critical point set's peaks, passes, pales, and pits can be relabeled in inverse order to produce a dual critical net. We note that the diamond structure critical nets shown in Fig. 5.3 are self dual in that there is mirror symmetry relating the top and bottom halves of the critical nets. The face-centered cubic critical nets in Fig. 5.2 and the body-centered cubic critical nets in Fig. 5.1 are not self dual; consequently we can turn those critical nets upside down to produce different families of critical nets.

The bottom two critical-net drawings in Fig. 5.4 illustrate the duality of graphite and hexagonal diamond. Note that the coordination vector (4)(4,2,6,6,2,4)(4) is identical to that for diamond in Fig. 5.3 while the summed multiplicity vector (16)(4,16,8,48,8,16,4)(16) is half that of diamond, which tells us there are more layers in real diamond but the averaged local topology is identical.

The x and z values given under the critical net in Fig. 5.4 provide the variable position parameters for occupied univariate and divariate Wyckoff sites. We felt it necessary to make some slight metric adjustment in going from graphite to hexagonal diamond based on empirical inspection of stereoscopic ORTEP diagrams. We have not done any analytical positioning of critical points based on the Gaussian density Morse function calculations since for most simple examples studied to date except basic beryllium acetate, the space groups usually provide enough fixed points to define the critical net details. That will not be the case for more complex crystal structure problems where many of the critical points are on general rather than special positions.

5.7 Critical Nets Versus Dirichlet Partitioning

Dirichlet partitioning of 3-space around a lattice-complex point is carried out by placing planes normal to vectors between neighboring points of the complex at midpoints of the vectors. This forms a convex polyhedron around the origin site in which all points within the polyhedron are closer to the origin site than to any other site of the complex. The vertices of a Dirichlet polyhedron are sometimes called interstices, implying holes between spherical atoms.

For the invariant lattice complex P, which represents simple cubic packing, the center, face, edge, and vertex barycenters (centroids) fall on the peak, pass, pale, and pit critical points of the critical net, respectively, as expected. For the body-centered lattice complex I, this correlation does not hold since the bcc peaks, passes, pales, and pits are on the center, 8 hexagonal faces, 24 vertices, and 6 square faces, respectively, rather than on the center, 14 faces, 36 edges, and 24 vertices of the bcc truncated octahedron Dirichlet polyhedron.

Because of such discrepancies, we recommend that critical nets be used in place of Dirichlet polyhedra tiling when practical. The Dirichlet partitioning algorithm is not based on Morse theory topology principles. Thus the bcc rhombohedral dodecahedron coordination polyhedron (12 faces, 24 edges, 14 vertices) is not dual to the bcc truncated octahedron Dirichlet polyhedron,[46] and it serves as a classic counterexample to the postulated duality between corresponding coordination and Dirichlet polyhedra, which the unwary may assume to be present.

6. Where do we go from here?

Since there is little crystallographic background literature available to provide guidance for future research, we present our list of research needs in crystallographic topology. The current state of the art can only be characterized as exploratory. As Walt Kelly's comic strip character Pogo once said, "We are faced with insurmountable opportunities."

6.1 Interpretation of Macromolecule Electron Density Maps

We first got into crystallographic topology in 1976 using critical point analysis as a representation method for heuristic reasoning interpretation of protein electron density maps.[39] The ORCRIT computer program we wrote at that time was "decommissioned" for 15 years but has recently been reactivated and used successfully in a series of feasibility study by Janice Glasgow, Suzanne Fortier, and their Queens' University colleagues.[47] The ORCRIT program is more oriented toward numerical analysis (i.e., 3-D linear blending interpolation and Newton iteration) and graph theory (i.e., minimal spanning trees) than topology. It uses only the peak and pass critical points to construct what might be called ridge lines which tend to trace the polymeric backbone and sidechains.

If we rewrite ORCRIT today, we would use Eric Grosse's spectral spline method[48] to find the critical point set, then numerically trace the separatrices. From the resulting critical net we can determine volume, integrated density, and topological shape descriptors for the chemical cages for computational comparison with related archived peptide and protein structure results. ORCRIT relied entirely on distance, angle, and critical-point eigenvector metric details, which are intrinsically less robust than integrated quantities and topological descriptors.

6.2 Critical Net Software Needs

We need to develop computer programs to determine routine critical nets for small molecule crystal structures such as basic beryllium acetate, shown in Fig. 3.5. We present a "wish list" of what we would like to develop or see developed by others. We need to:

- Write a modified ORCRIT program that, through summation of crystal space Gaussian density functions, can calculate density and its first two derivatives at any point in an asymmetric unit. ORCRIT can then do its pattern search for critical points without storing or interpolating density maps on grids.
- Write a "twisted H" search function for ORTEP based on the comments in Sect. 3.9 to assign critical net indices and separatrices.
- Modify ORTEP-III to more automatically plot critical net drawing given the critical points and separatrices. The current features are minimal.
- Write a matroid[49] program to resolve hierarchically the orbifold singular set in one direction and the crystal structure critical net in a second direction. Such a program could provide a representation for crystal structure classification, archiving, and querying. This "dimatroid" could also serve as a "blackboard representation" in heuristic programming for stepwise conversions of $Fd\bar{3}$ (in Fig. 5.3) to the full basic beryllium acetate critical graph, for example.

6.3 Orbifold Atlas

The orbifold atlas we have mentioned several times is needed for both pedagogical and research reference purposes. For each space group the atlas might include two identical orbifold singular sets drawings with Wyckoff site symbols on one and lattice complex plus axis order numbers symbols on the other. Perhaps the simplest possible linearized critical net graph(s) for that space group might also be presented. There should also be a list of coordinates for the fundamental domain (asymmetric unit) vertices used based on the ITCr[1] space group drawing selected. A brief description of the underlying topological space and the key orbifolding steps used to close the fundamental domain should also be included.

In addition to a sequential ordering of orbifolds based on the standard space group numbers, subgroup/lattice-complex trees of linearized critical net graphs such as Figs. 5.1, 5.2, and 5.3 could be made for the various crystal families. A nomenclature system based on such graphs would be useful in crystal structure classification.

Graphics automation of singular set drawing would certainly be welcome and perhaps essential since the existing computer-assisted drawing programs such as Adobe Illustrator are very labor intensive when applied to this task. One approach is to use a graphics techniques of knot theory where Möbius energy functions based on Coulomb's law are applied to space curves, links, knotted graphs, surfaces, and other submanifolds.[50] Programs such as Scharein's KnotPlot, Brakke's Surface Evolver and the Geometry Center's GeomView, which are all described on the World Wide Web, might be adapted to this task.

6.4 Interactive Data Base for Space Groups and Orbifolds

Existing commercial space group data base programs have not been useful in our research. We would like to see a noncommercial World Wide Web site that provides the key information of the ITCr[1] for any space group including Wyckoff sites and subgroup family data. An interactive orbifold atlas could be implemented through addition of database retrieval for topological orbifold data.

The computer algebra system GAP,[51] which stands for Groups, Algebra and Programming, was developed by Joachim Neubueser and coworkers of Lehrstuhl D für Mathematik, RWTH, Aachen, Germany. GAP now contains a crystallographic library for two, three, and four dimensional space groups based on the tables of Brown *et al*.[52] A WWW server might be feasible that would combine orbifold data bases and the GAP system to provide interactive answers to both standard and research level inquiries about crystallographic groups and orbifolds.

6.5 Orbifold Covers Based on Color Groups

The bicolor Shubnikov space groups and other crystallographic color groups[26] have both symmetry and antisymmetry group elements with the symmetry elements carrying out the normal positional transformation operations. The antisymmetry elements of an n-color group are essentially the elements of a group that are deleted in going from a group to one of its index-n normal subgroups. The color groups are often used in crystal physics applications such as the description of magnetic patterns in crystal structures, but they can be used here to describe the cover of an orbifold or to derive one Euclidean 3-orbifold from another 3-orbifold when their parent space groups have a group/n-index normal subgroup relationship.

We have derived graphical representations for the 58 bicolor spherical 2-orbifolds to supplement Fig. 2.3 and it would not be difficult to extend this to the bicolor plane groups. Full bicolor illustrations of the 1191 nontrivial Shubnikov space groups are given in Koptsik[53] but the complexity of those illustrations is quite overwhelming. An atlas of Euclidean bicolor 3-orbifold drawings is perhaps feasible but not a trivial project.

Using GAP, it should be possible to rederive the Shubnikov space groups computationally and from them derive the ordinary Euclidean 3-orbifolds in space group/subgroup families starting from a small number of top level orbifolds in each family derived with normal geometric topology cut-and-paste methods.

6.6 Analytical Topology

Although there is a huge analytical topology literature that should seemingly be applicable to crystallographic topology problems, the only equation that we have found really useful in practice is the Euler-Poincare equation, which states that the alternating sum for the numbers of the sequential critical point types is zero for Euclidean manifolds of all dimensions. We need equivariant invariants for characterization of orbifolds, underlying topological spaces of orbifolds, and crystallographic Morse functions on space groups and orbifolds. We anticipate that such invariants probably involve cohomology.[7,31,32,33]

Thurston[16,17,54] conjectures that each closed 3-manifold can be decomposed (by connected sums and splitting along incompressible tori) into pieces, each of which has a geometric structure modeled on one of eight types of 3-dimensional geometries—H^3, Sol, S^3, E^3, $S^2 \times R$, $H^2 \times R$, Nil, and (the universal cover of) SL(2,R). Structures on Seifert manifolds account for the last six of the eight geometries. Several of the underlying spaces for orientable 3-orbifolds have S^3 (for dihedral point groups) and $S^2 \times R$ (for cyclic point groups) as underlying spaces, and the 10 Euclidean manifolds have Seifert manifolds as underlying spaces. Are there any formal theorems that give all the underlying spaces for Euclidean 3-orbifolds in terms of specific classes of geometries or manifolds?

At times we need to trace geodesic paths in orbifolds corresponding to general straight lines in Euclidean crystal space. For Euclidean and spherical 2-orbifolds, conformal mapping, using the Schwarz-Christoffel transformation from an arbitrary circle or half plane (orbifold) to an n-gon (fundamental domain), and analytic continuation, based on Schwartz's principle of reflection, will work assuming the reverse transformation also is available. However, our problems are mainly 3- rather than 2-dimensional. The literature on Riemannian orbifolds (e.g., Riemannian geometry of orbifolds[55]) should be followed for its relevance to this problem.

Appendix

The 36 cubic crystallographic space groups are different from the remaining 194 space groups in that they each have body diagonal 3-fold axes arising from their tetrahedral and octahedral point groups. These body diagonal 3-fold axes make their orbifolds a less understood topology problem in that the Siefert fibered spaces approach of lifting from a base Euclidean 2-orbifold is inapplicable since fibration along the required orthogonal projections become tangled together by the 3-fold axes. On the other hand, many aspects of the cubic groups orbifolds are more straightforward than for the simpler space groups that are based on cyclic and dihedral point groups.

The 36 Euclidean 3-orbifolds for the cubic space groups (i.e., the cubic 3-orbifolds) are illustrated in Figs. 2.8 of Sect. 2 and A.1 of this Appendix. The 12 cubic 3-orbifolds in Fig. 2.8 have S^3 as their underlying topological space. For the 24 cubic orbifolds in Fig. A.1, the first 11 have a 3-ball underlying space, the next two have singly suspended projective 2-planes (RP^2) with mirror boundary, followed by 10 with doubly suspended projective 2-planes (RP^2). The final cubic 3-orbifold in Fig. A.1 has a projective 3-plane (RP^3) underlying space.

The small circles at the points of each projective plane cone in Fig. A.1 denote projective plane suspension points which arise from mirror-free inversion centers of the space groups. The dashed lines around the circumference denote the antipodal relationship for points halfway around each circle on the cone surface. The dashed line around the RP^3 sphere denotes an antipodal gluing relationship for all points on any great circle of the RP^3 spherical representation. Orbifolds having an RP^2 or RP^3 underlying space may be drawn in several different ways because of the sliding antipodal gluing relationship for projective planes discussed in Sect. 2. For the RP^2 examples in Fig. A.1, drawings with the least possible number of singular-set components on the antipodal surface are shown. The symbols at the vertices of the singular set graphs in the orbifolds denote invariant lattice complexes defined in Sect. 5. An extension of this notation to describe the complete orbifold for $I\bar{4}3m$ (#217) is given in Sect. 5.3.

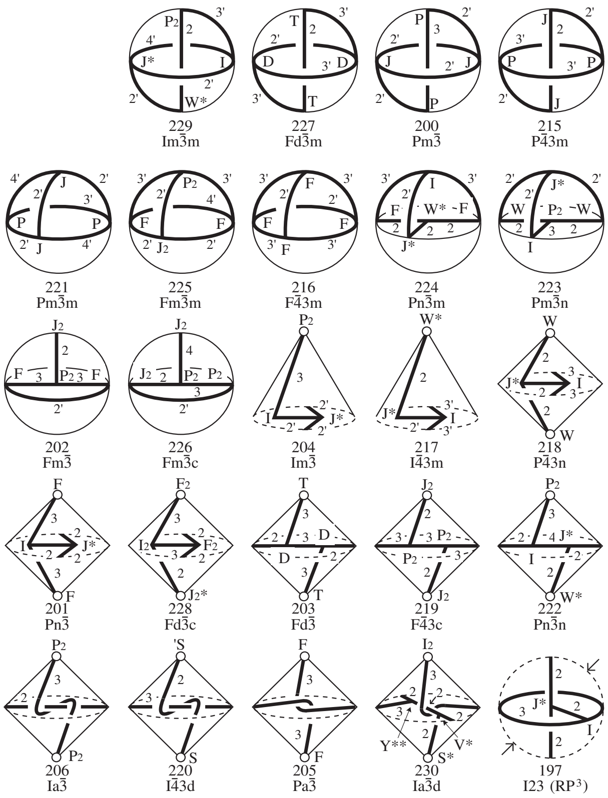

Figure A.1. The 24 cubic 3-orbifolds that do not have S^3 as the underlying topological space.

Each cubic group has an index-4 rhombohedral based trigonal subgroup and an index-3 orthorhombic or tetragonal subgroup. There are only seven rhombohedral space groups: R3 (3), R32 (32), $R\bar{3}m$ and $R\bar{3}c$ ($\bar{3}m$), R3m and R3c (3m), and $R\bar{3}$ ($\bar{3}$) where the symbol in parentheses is the corresponding trigonal point group. Thus it seemed a reasonable approach to order the cubic groups in columns according to their index-4 rhombohedral subgroups and in rows according to their index-2 cubic subgroups. After some additional partitioning of $R\bar{3}m$ and $R\bar{3}c$ columns we arrived at the subgroup graph shown in Fig A.2. We thank John H. Conway of Princeton for an e-mail exchange explaining his related "odd-subroutine" approach to the group classification problem that he has applied to a number of group classification problems including the crystallographic space groups.

Fig. A.2 uses the subgroup, group normalizer, and lattice complex information given in the ITCr.[1] Each box contains the cubic space group symbol in the upper right subbox, the index-3 orthorhombic or tetrahedral subgroup in the middle, and their respective ITCr sequence numbers on the bottom line. The upper left subbox contains the simplest lattice complex of the cubic space group. Orbifolds for the index-3 subgroups of the cubic groups can be used to derive the cubic orbifolds. Boldface type identifies group normalizers, and group normalizer basins are identified by bold solid lines leading down from cubic (but not orthorhombic) group normalizers.

The seven rhombohedral trigonal subgroups of the cubic groups are shown in the bottom row of the figure with their space group symbols and simplest lattice complex in the top row of each box. The index-3 subgroups (monoclinic/triclinic) of the rhombohedral groups are indicated on the middle line and the respective ITCr numbers on the bottom line of each box. The divider strip between the cubic and rhombohedral groups gives the point groups for all the space groups involved in each column, with the cubic/orthorhombic (or tetragonal) to the left and the rhombohedral/monoclinic (or triclinic) to the right.

Two boxes in a row that are not separated by a space belong to a specific column. To minimize clutter in the drawing we use the convention that whenever a subgroup connection line goes to the midline separating adjacent boxes, both boxes are involved in the subgroup relation. If that line goes to another pair of adjoined boxes, the right goes to the right and the left to the left except when there is a loop in the subgroup relation line, which indicates a right-left interchange. All solid lines join order-2 subgroups and pertain to the cubic, orthorhombic/tetragonal, rhombohedral, and monoclinic/triclinic sets of groups individually. The orthorhombic space group set forms pairs of duplicates.

The dashed lines leading to a dashed box two levels further down is an index-4 subgroup relationship. Note that each dashed box is a repeat of the regular box three levels up in the same column, reflecting the Bravais lattice repetition I, P, F, I, P which occurs in each column as denoted by the initial letters in the space group symbols. This relationship only holds for the cubic space groups in the figure and not for the orthorhombics/tetragonals. Since Fig. A.2 is meant to be used mainly for orbifold applications, it does not include explicit information on how many unit cells are required for each space group/subgroup relationship.

Note that for order-2 subgroups, there are two independent cubic space group families, one starting at $Im\bar{3}m$ and ending at F23, and the second starting at $Ia\bar{3}d$ and ending at $P2_13$. The ending space groups are the only two cases of space groups without order-2 subgroups. The two series are sometimes called the A and B cubic space group families, respectively.

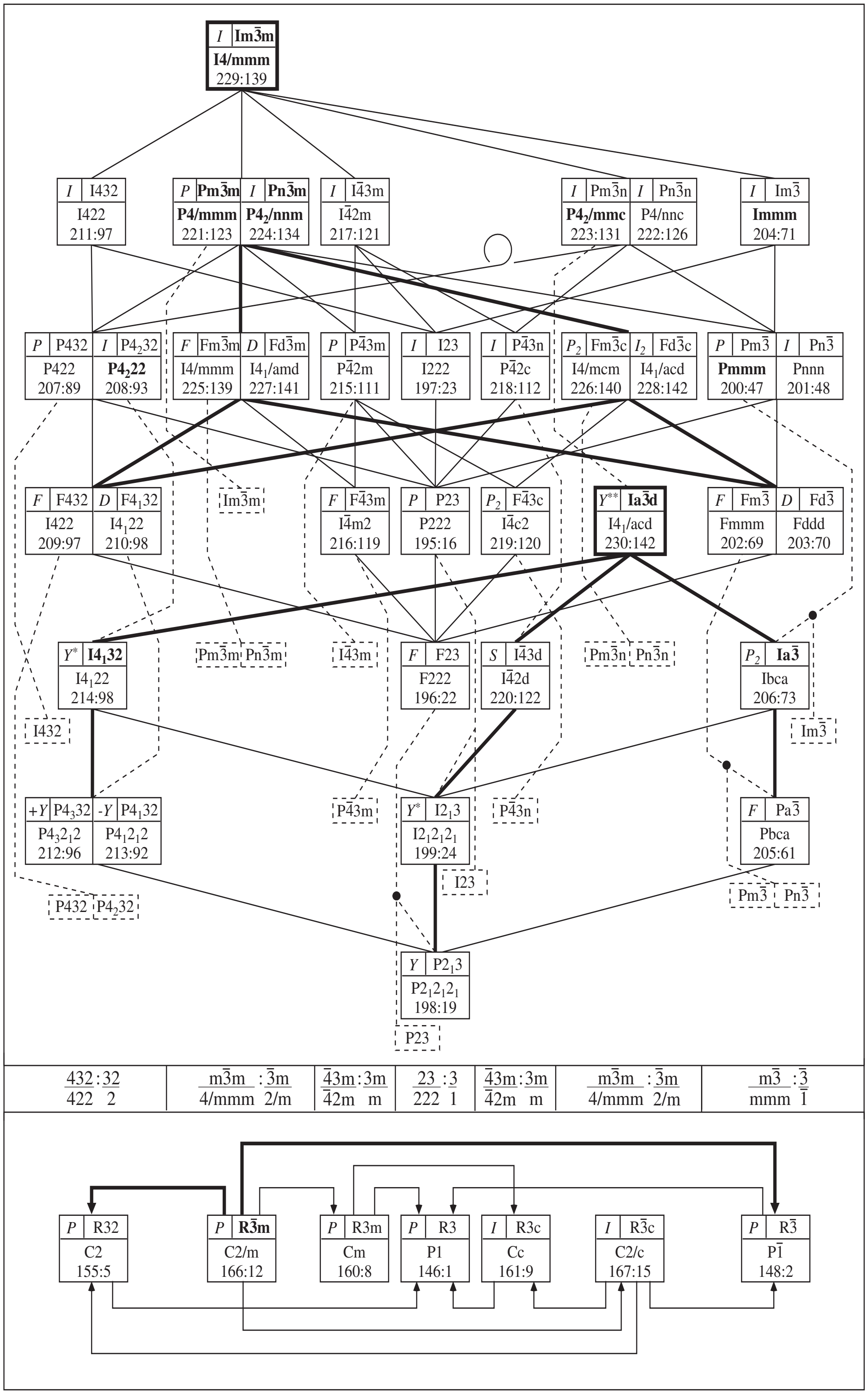

Figure A.2. Cubic space group/subgroup graph.

Solid lines = index 2; dashed lines and rhombohedral column subgroups = index 4; space groups in lower parts of boxes = index 3.

References

[1] T. Hahn, ed., *International Tables for Crystallography, Volume A: Space-Group Symmetry*, Kluwer Academic Publishers, Dordrecht, The Netherlands, 1995.

[2] M. Morse and S. S. Cairns, *Critical Point Theory in Global Analysis and Differential Topology: An Introduction*, Academic Press, 1969.

[3] J. Milnor, *Morse Theory*, Princeton University Press, Princeton, New Jersey, 1969.

[4] M. Goresky and R. MacPherson, "Stratified Morse Theory" in *Proc. Symp. Pure Math.*, Vol. 40, pp. 517-533, 1983; M. Goresky and R. MacPherson, Stratified Morse Theory, Springer-Verlag, New York, 1988.

[5] L. E. El'sgol'c, *Qualitative Methods in Mathematical Analysis*, American Mathematical Society, Providence, Rhode Island, 1964.

[6] M. N. Burnett and C. K. Johnson, *ORTEP-III: Oak Ridge Thermal Ellipsoid Plot Program for Crystal Structure Illustrations*, ORNL-6895, Oak Ridge National Laboratory, 1996.

[7] A. Dimca, *Singularities and Topology of Hypersurfaces*, Springer-Verlag, New York, 1992.

[8] C. T. C. Wall, "Deformations of Real Singularities," *Topology*, Vol. 29, pp. 441-460, 1990.

[9] R. F. W. Bader, *Atoms in Molecules—A Quantum Theory*, University Press, Oxford, 1991.

[10] S. Barr, *Experiments in Topology*, Dover Publications, Inc., New York, 1964.

[11] G. McCarty, *Topology: An Introduction with Application to Topological Groups*, Dover Publications, Inc., New York, 1967.

[12] D. Rolfsen, *Knots and Links*, Publish or Perish, Inc., Houston, Texas, 1990.

[13] L. C. Kinsey, *Topology of Surfaces*, Springer-Verlag, New York, 1993.

[14] K. Ito, ed., *Encyclopedic Dictionary of Mathematics*, Second Ed., The MIT Press, Cambridge, Massachusetts, 1987.

[15] I. Satake, "On a Generalization of the Notion of a Manifold," *Proc. Nat. Acad. of Science USA*, Vol. 42, pp. 359-363, 1956.

[16] W. P. Thurston, "Three-Dimensional Geometry and Topology," The Geometry Center, University of Minnesota, 1992.

[17] P. Scott, "The Geometry of 3-Manifolds," *Bull. Lond. Math. Soc.*, Vol. 15, pp. 401-487, 1983.

[18] W. D. Dunbar, "Fibered Orbifolds and Crystallographic Groups," Ph.D. Dissertation, Princeton University, 1981.

[19] W. D. Dunbar, "Geometric Orbifolds," *Rev. Mat. Univ. Comp. Madrid*, Vol. 1, pp. 67-99, 1988.

[20] F. Bonahon and L. Siebenmann, "Seifert 3-Orbifolds and Their Role as Natural Crystalline Parts of Arbitrary Compact Irreducible 3-Orbifolds," unpublished, 1983.

[21] F. Bonahon and L. Siebenmann, "The Classification of Seifert Fibered 3-Orbifolds" in *Low Dimensional Topology*, Cambridge University Press, pp. 19-85, 1985.

[22] J. M. Montesinos, *Classical Tessellations and Three-Manifolds*, Springer-Verlag, New York, 1987.

[23] J. H. Conway, "The Orbifold Notation for Surface Groups" in *Groups, Combinatorics & Geometry*, M. Liebeck and J. Saxl, eds., Cambridge University Press, pp. 438-447, 1992.

[24] J. Conway and B. Thurston, "Two and Three-Dimensional Euclidean Orbifold Voodoo," preprint.

[25] W. S. Massey, *Algebraic Topology: An Introduction*, Springer-Verlag, New York, pp. 145-180, 1967.

[26] R. L. E. Schwartzenberger, "Colour Symmetry," *Bull. London Math. Soc.*, Vol. 16, pp. 209-240, 1984.

[27] P. Orlik, *Seifert Manifolds*, Springer-Verlag, New York, 1972.

[28] J. A. Wolf, *Spaces of Constant Curvature*, 5th Ed., Publish or Perish, Inc., Wilmington, Delaware, 1984.

[29] C. K. Johnson and H. A. Levy, "Thermal-Motion Analysis Using Bragg Diffraction Data," *International Tables for X-Ray Crystallography, Volume IV*, J. A. Ibers and W. C. Hamilton, eds., The Kynoch Press, Birmingham, England, pp. 311-334, 1974.

[30] L. van Hove, "The Occurrence of Singularities in the Elastic Frequency Distribution of a Crystal," *Phys. Rev.*, Vol. 89, pp. 1189-1193, 1953.

[31] E. Bierstone, *The Structure of Orbit Spaces and the Singularities of Equivariant Mappings*, Instituto de Matematica Pura e Aplicada, Rio de Janeiro, 1980.

[32] E. Lerman and S. Tolman, "Hamiltonian Torus Actions on Symplectic Orbifolds and Toric Varieties," Differential Geometry Preprint #dg-ga/9511008, 1995.

[33] F. C. Kirwan, *Cohomology of Quotients in Symplectic and Algebraic Geometry*, Princeton University Press, Princeton, New Jersey, 1984.

[34] A. W. M. Dress, D. H. Huson and E. Molnár, "The Classification of Face-Transitive Periodic Three-Dimensional Tilings," *Acta Cryst.*, Vol. A49, pp. 806-817, 1993.

[35] E. Molnár, "Symmetry Breaking of the Cube Tiling and the Spatial Chess Board by D-Symbols," *Algebra and Geometry*, Vol. 35, pp. 205-238, 1994.

[36] O. Delgado Friedrichs and D. H. Huson, "Orbifold Triangulations and Crystallographic Groups," *Period. Math. Hung.*, in press.

[37] F. P. Bundy and J. S. Kasper, "Hexagonal Diamond—A New Form of Carbon," *J. Chem. Phys.*, Vol. 46, pp. 3437-3446, 1967.

[38] A. Tulinsky, C. R. Worthington, and E. Pignataro, "Basic Beryllium Acetate: Parts I-III," *Acta Cryst.*, Vol. 12, pp. 623-637, 1959.

[39] C. K. Johnson and E. Grosse, "Interpolation Polynomials, Minimal Spanning Trees and Ridge-Line Analysis in Density Map Interpretation," *Abstracts of the American Crystallographic Association Meeting, Evanston, Illinois, Aug. 9-12, 1976*; C. K. Johnson, "Peaks, Passes, Pales, and Pits: A Tour through the Critical Points of Interest in a Density Map," *Abstracts of the American Crystallographic Association Meeting, Pacific Grove, California, Feb. 21-25, 1977*.

[40] E. Hellner, "Descriptive Symbols for Crystal-Structure Types and Homeotypes Based on Lattice Complexes," *Acta Cryst.*, Vol. 19, pp. 703-712, 1965.

[41] W. Fisher, H. Burzlaff, E. Hellner, and J. D. J. Donnay, *Space Groups and Lattice Complexes*, National Bureau of Standards Monograph 134, 1973.

[42] E. Koch, "A Geometrical Classification of Cubic Point Configurations," *Z. Krist.*, Vol. 166, pp. 23-52, 1984.

[43] W. Fischer and E. Koch, "Lattice Complexes," pp. 825-854 in *International Tables for Crystallography, Volume*

A, T. Hahn, ed., Kluwer Academic Publishers, Dordrecht, The Netherlands, 1995.

[44] E. Hellner, E. Koch, and A. Reinhardt, *The Homogeneous Frameworks of the Cubic Crystal Structures, Physics Data*, Nr. 16-2, 1981.

[45] E. Koch and W. Fischer, “Lattice Complexes and Limiting Complexes Versus Orbit Types and Non-characteristic Orbits: a Comparative Discussion,” *Acta Cryst.*, Vol. A41, pp. 421-426, 1985.

[46] A. L. Loeb, “A Systematic Survey of Cubic Crystal Structures,” *J. Solid State Chem.*, Vol. 1, pp. 237-267, 1970.

[47] L. Leherte, S. Fortier, J. Glasgow, and F. H. Allen, “Molecular Scene Analysis: Application of a Topological Approach to the Automated Interpretation of Protein Electron Density Maps,” *Acta Cryst.*, Vol. D50, pp. 155-166, 1994.

[48] E. H. Grosse, “Approximation and Optimization of Electron Density Maps,” Ph.D. Dissertation, Stanford University, Stanford, California, 1980.

[49] A. Björner, M. Las Vergnas, B. Sturmfels, N. White, and G. M. Ziegler, *Oriented Matroids, Encyclopedia of Mathematics*, Vol. 46, Cambridge University Press, Cambridge, England, 1993; G. M. Ziegler, “Oriented Matroids Today,” World Wide Web http://www.math.tu-berlin.de/~ziegler, 1996.

[50] R. B. Kusner and J. M. Sullivan, “Möbius Energies for Knots and Links, Surfaces and Submanifolds,” preprint, 1994.

[51] Martin Schönert *et al.*, *GAP—Groups, Algorithms, and Programming*, Lehrstuhl D für Mathematik, Rheinisch Westfälische Technische Hochschule, Aachen, Germany, first edition, 1992.

[52] H. Brown *et al.*, *Crystallographic Groups of Four-Dimensional Space*, John Wiley & Sons, New York, 1978.

[53] V. A. Koptsik, *Shubnikov Groups*, Izd. MGU, Moscow, pp. 212-227, 1966.

[54] W. P. Thurston, “Three-Dimensional Manifolds, Kleinian Groups, and Hyperbolic Manifolds,” *Bull. Amer. Math. Soc.*, Vol. 6, pp. 357-382, 1982.

[55] J. E. Borzellino, “Riemannian Geometry of Orbifolds,” Ph.D. Dissertation, University of California, Los Angeles, 1992.